HHS Public Access

Author manuscript

*Hum Brain Mapp*. Author manuscript; available in PMC 2018 June 01.

Published in final edited form as:

*Hum Brain Mapp*. 2017 June ; 38(6): 3098–3112. doi:10.1002/hbm.23577.

以有癫痫病史的孩子做对照组

脑电和代谢

# Objective 3D Surface Evaluation of Intracranial Electrophysiologic Correlates of Cerebral Glucose Metabolic Abnormalities in Children with Focal Epilepsy

**Jeong-Won Jeong**[1,2], **Eishi Asano**[1], **Vinod Kumar Pilli**[1,2], **Yasuo Nakai**[1], **Harry T. Chugani**[3,4], and **Csaba Juhász**[1,2]

[1]Departments of Pediatrics and Neurology, School of Medicine, Wayne State University, Detroit, MI, USA

[2]Translational Imaging Laboratory, PET Center, Children's Hospital of Michigan, Detroit, MI, USA

[3]Department of Neurology, Nemours DuPont Hospital for Children, Wilmington, DE, USA

[4]Thomas Jefferson University School of Medicine, Philadelphia, PA, USA

## Abstract

To determine the spatial relationship between 2-deoxy-2[$^{18}$F]fluoro-D-glucose (FDG) metabolic and intracranial electrophysiological abnormalities in children undergoing two-stage epilepsy surgery, we used statistical parametric mapping (SPM) to correlate hypo- and hypermetabolic cortical regions with ictal and interictal electrocorticography (ECoG) changes mapped onto the brain surface. Preoperative FDG-PET scans of 37 children with intractable epilepsy (31 with non-localizing MRI) were compared to age-matched pseudo-normal pediatric control PET data. Hypo-/hypermetabolic maps were transformed to 3D-MRI brain surface to compare the locations of metabolic changes with electrode coordinates of the ECoG-defined seizure onset zone (SOZ) and interictal spiking. While hypometabolic clusters showed a good agreement with the SOZ on the lobar level (sensitivity/specificity=0.74/0.64), detailed surface-distance analysis demonstrated that large portions of ECoG-defined SOZ and interictal spiking area were located at least 3cm beyond hypometabolic regions with the same statistical threshold (sensitivity/specificity=0.18–0.25/0.94–0.90 for overlap-3cm distance); for a lower threshold, sensitivity for SOZ at 3cm increased to 0.39 with a modest compromise of specificity. Performance of FDG-PET SPM was slightly better in children with smaller as compared to widespread SOZ. The results demonstrate that SPM utilizing age-matched pseudocontrols can reliably detect the lobe of seizure onset. However, the spatial mismatch between metabolic and EEG epileptiform abnormalities indicates that a more complete SOZ detection could be achieved by extending intracranial electrode coverage at least 3cm beyond the metabolic abnormality. Considering that the extent of feasible electrode coverage is limited, localization information from other modalities is particularly important to optimize grid coverage in cases of large hypometabolic cortex.

Corresponding author: Jeong-Won Jeong, PhD., Departments of Pediatrics and Neurology, Wayne State University School of Medicine, PET Center and Translational Imaging Laboratory, Children's Hospital of Michigan, 3901 Beaubien St., Detroit, MI, 48201, Phone: 313-993-0258; Fax: 313-966-9228; jeongwon@pet.wayne.edu.

The authors declare no conflicts of interest.

**Keywords**

FDG PET; SPM; pediatric epilepsy; Epilepsy surgery; electrocorticography; seizure onset

## Introduction

By definition, the epileptogenic zone is the cortical region whose resection is necessary and sufficient to achieve seizure freedom, however, none of the currently available diagnostic markers can optimally delineate the epileptogenic zone [Rosenow et al., 2001; Asano et al., 2013]. To best estimate the location of the epileptogenic zone in the presurgical evaluation of drug-resistant pediatric epilepsy, clinicians often monitor intracranial electrocorticography (ECoG) activity from the affected hemisphere. Thereby, the seizure onset zone (SOZ) responsible for the habitual seizures is generally considered to be a critical part of the epileptogenic zone [Asano et al., 2009; Fuiwara et al., 2012; Weiss et al., 2015]. Between seizure events, interictal spike discharges are often generated by SOZ and surrounding cortex; thus, such interictal spikes can also be used to predict the epileptogenic zone [Palmini et al., 1995; Asano et al., 2013]. The aforementioned ECoG measures are useful presumably only when intracranial electrodes satisfactorily sample the true epileptogenic zone [Widdess-Walsh et al., 2007]. Thus, noninvasive modality accurately guiding intracranial electrode placement is highly desired by those practicing epilepsy surgery.

Positron emission tomography (PET) of the brain with 2-deoxy-2[$^{18}$F]fluoro-D-glucose (FDG) plays an important role in noninvasively estimating the location of the epileptogenic zone [Kumar et al., 2010; Stanescu et al., 2013]. FDG-PET is widely used for pediatric populations [de Silva et al., 1997; Hader et al., 2004; Kumar et al., 2010; Stanescu et al., 2013], especially when MRI is non-localizing. According to previous PET studies assessed on a non-statistical basis, the accuracy of the metabolic abnormality to localize the SOZ or interictal spiking area on ECoG has been suboptimal [Hong et al., 2002; Juhász et al., 2001]. Specifically, our previous studies demonstrated a metabolic-electrophysiologic mismatch in extent between areas of focal glucose hypometabolism and ECoG-defined SOZ [Juhász et al., 2000; Alkonyi et al., 2009].

PET image analysis is mostly based on visual assessment in the clinical setting. Research studies used a variety of quantitative approaches, but comparison across centers is difficult without statistically defining the metabolic abnormalities. Overall, the lack of a standardized image analysis approach across centers makes it difficult to compare data in the literature or create clear guidelines based on class I-II evidence [Jayakar et al., 2014]. This issue may account for the variable performance of FDG-PET reported in the literature [Juhasz et al., 2012].

To overcome this problem, statistical parametric mapping (SPM) analysis of PET images has been investigated for about two decades. SPM is an objective, quantitative, and observer-independent method to identify metabolic abnormalities in whole brain using general linear model and Gaussian random field theory [Friston et al., 1996; Kim et al., 2003]; however, this approach requires comparison to a control PET data set that is impossible to obtain in

healthy children for ethical reasons, especially in young children. Therefore, pediatric SPM studies often applied a young adult healthy control group, but this approach has only been validated in children age 6 years and above [Muzik et al., 2000; Kumar et al., 2010]. An alternative approach for SPM analysis of pediatric PET images is the use of a "pseudo-control" pediatric group, i.e., carefully selected PET scans of epileptic children showing a normal metabolic pattern by visual assessment. This concept was originally introduced by Chugani et al. [1986; 1987], who demonstrated that such PET images are able to characterize global and regional maturational changes in normal human brain glucose metabolism. A recent study by another group [Archambaud et al., 2013] showed that the use of such a pseudo-control group can also improve specificity of detecting brain metabolic abnormalities in objective PET studies using SPM in children with drug-resistant epilepsy. The pseudo-control group in that study was relatively small (n=24) and included only children 4.5 years of age and above. To our best knowledge, no study has validated the potential use of SPM to detect FDG-PET abnormalities epileptic in children below 4. 5 years of age.

In the present study, our key hypothesis was that the use of carefully selected age-matched pseudo-control PET data may provide comparable accuracy in detecting ECoG-defined SOZ across a wide age range, including children as young as 1 year of age. For this analysis, we utilized a large pseudo-control pediatric PET group, including epileptic children with a wide age range (1–18 years) and normal (by visual inspection) glucose metabolic pattern on PET. Using this group, we aimed at optimizing the accurate detection of regional glucose metabolic abnormalities in a pediatric epilepsy group, using SPM. In addition, we tested the feasibility of a 3D surface mapping analysis, which visualizes SPM-defined metabolic abnormalities in native anatomical brain surface generated by FreeSurfer analysis [Fishl et al., 2001; Fishl et al., 2004] in order to perform a direct spatial comparison between ECoG-defined epileptic cortex and areas of abnormal glucose metabolism defined objectively by SPM.

To study the spatial association of ECoG-defined SOZ and metabolic abnormalities in detail, we performed a comparative PET/ECoG analysis with various statistical thresholds and Euclidean distances in children with focal epilepsy (mostly with non-localizing MRI) who underwent two-stage epilepsy surgery with extensive subdural electrode coverage. We also analyzed whether this analysis provides consistent performance in various patient subgroups depending on age, epilepsy duration, extent of epileptic cortex and surgical outcome.

## Methods

### Subjects

Thirty-seven children (age: 9.7±5.2 years, 1.2–18.7 years; 20 girls) with intractable focal neocortical epilepsy of both temporal and extratemporal origin (22 with left-, 15 with right-hemispheric SOZ) who underwent two-stage epilepsy surgery at the Children's Hospital of Michigan (Detroit) between 2008 and 2015 were included in the study. The summary of clinical and demographic profiles of these children is given in Table 1. The inclusion criteria consisted of age between 1 and 19 years; detailed presurgical evaluation, including interictal FDG-PET, followed by two-stage epilepsy surgery with chronic subdural ECoG monitoring;

at least one year of postsurgical follow-up. The exclusion criteria were MRI diagnosis of major hemispheric deformity such as hemimegalencephaly, perisylvian polymicrogyria, and porencephaly, as well as hemispherectomy, and history of prior epilepsy surgery.

On the basis of chronic subdural ECoG data, ictal seizure onset was localized in 1–4 lobes (Table 1). MRI showed a focal cortical abnormality in 6 children, including 2 with tuberous sclerosis complex, 2 with low-grade tumors, and 2 with signal abnormalities consistent with gliosis or cortical dysplasia. Histology results are shown in Table 1.

The control group for SPM analysis of FDG-PET scans included 64 children (age: 9.3±5.2 years, 1–18 years; 31 girls) with a history of epilepsy. Briefly, from a pediatric database of 1,500 PET scans acquired using a single PET/CT scanner and an identical scanning protocol at the Children's Hospital of Michigan (Detroit) between 2006 and 2013, we first identified 185 scans reported to have a normal glucose metabolic pattern on the original clinical PET report generated by a single investigator (HTC). After reviewing electro-clinical data, MRI and PET images of these 185 patients, we identified 64 children who met the following criteria: 1) normal glucose metabolic pattern on PET, including lack of significant asymmetries, focal decreases or increases, or global cortical changes by visual assessment, 2) **no seizure(s) during the PET scan confirmed by the clinical observation and scalp EEG monitored during the FDG uptake period**, 3) no MRI lesion, and 4) no history of developmental delay. None of these 64 children underwent subsequent epilepsy surgery.

All participants were studied according to the guidelines of the Human Investigation Committee of Wayne State University. Written informed consent was obtained from the parents or legal guardians of the children who underwent epilepsy surgery. In addition, the Human Investigations Committee at Wayne State University granted permission for the retrieval and analysis of the clinical and imaging (including PET) data that had been obtained clinically for all children with a diagnosis of epilepsy.

## Data acquisition

All PET studies were performed using a GE Discovery STE PET/CT, located at Children's Hospital of Michigan. The scanner combines a Light-Speed 16-slice CT with an advanced BGO PET system yielding 47 image planes with a 16 cm axial field-of-view (FOV). The reconstructed image in-plane resolution is 5.5±0.35 mm at full-width-at-half-maximum (FWHM) and 6.0±0.49 mm in the axial direction (reconstruction parameters: Shepp-Logan filter with 0.3 cycles/pixel cutoff frequency). All subjects fasted for at least 6 hours prior to the PET procedure. EEG was monitored using surface electrodes during the entire FDG uptake period to ensure interictal scans. A venous line was established for tracer injection (0.141mCi/kg FDG). During the FDG uptake period external stimuli were minimized by dimming the lights and discouraging interaction so that studies reflected the resting awake state. Forty minutes after FDG injection, a static 20-minute emission scan of the brain was acquired in 3D mode.

As part of the clinical work-up, all children had an MRI including a high resolution T1 image acquired using a 3T GE-Signa scanner equipped with an 8-channel head coil and

ASSET at TR/TE/TI of 9.12/3.66/400ms, with a slice thickness of 1.2 mm, and planar resolution of 0.94×0.94 $mm^2$.

For the PET and MRI scanning period (but not during FDG uptake), most children were sedated with pentobarbital (1.5–3 mcg/kg) and midazolam (0.1–0.2 mcg/kg); or by midazolam (0.1 – 0.2 mcg/kg) followed by dexmedetomidine (1–2 mcg/kg), titrated slowly to achieve mild to moderate sedation. All sedated subjects were continuously monitored by a pediatric nurse, and physiological parameters (heart rate, pulse oximetry) were measured throughout the study.

Before surgery, all patients underwent standard presurgical evaluation, as described previously [Chugani et al., 2014]. In brief, all patients were evaluated with scalp ictal/interictal video-EEG, MRI, FDG-PET, and neuropsychological assessment. Subsequently, all cases were discussed in a weekly multidisciplinary epilepsy surgery conference where the results were reviewed. Based on this information (including visual PET assessment but not SPM data), subdural electrodes (10 mm intercontact distance, 4 mm diameter, Ad-Tech Medical) were implanted during Stage 1 of the two-stage surgery. Subdural ECoG was recorded for 3 to 5 days with a sampling rate at 1000 Hz. Grid, strip and/or depth electrodes were placed under the guidance of a board-certified clinical neurophysiologist (EA) near the regions suspected to be the epileptogenic zone. The number of implanted subdural macroelectrodes ranged from 90 to 160 per patient. **The averaged voltage of signals derived from the fifth and sixth intracranial electrodes of the amplifier was used as the original reference; signals were then re-montaged to a common average reference** [Crone et al., 2001; Canolty et al., 2006; Nagasawa et al., 2012; Sakuraba et al., 2016]. As a part of clinical evaluation, SOZ was defined as electrode site(s) initially showing sustaining rhythmic ECoG changes prior to the onset of clinical symptoms of the habitual seizures [Asano et al., 2009]. Interictal spike discharges, sharply-contoured waveforms standing out from the background rhythm which cannot be explained by physiological rhythms such as lambda or mu waves [Asano et al., 2009], were also detected by visual assessment. ‘Interictal spike zone’ was defined as the area(s) outside SOZ generating interictal spike discharges. In the present study, SOZ was the primary outcome measure, and ‘interictal spike zone’ was the secondary one. It should be noted that we did not place electrodes more than clinically indicated, and the clinical ECoG monitoring period was not extended for the purposes of the present study.

## Data analysis

FDG-PET image volumes were analyzed using the SPM8 software package (www.fil.ion.ucl.ac.uk/spm) to identify hypo-/hyper metabolic regions objectively while using age-matched pseudo-normal data in a voxel-by-voxel comparison. First, using SPM DARTEL procedure, pediatric age-specific FDG templates were created at five different age-ranges of the pseudo-normal controls, 1–3 years (n=14), 4–6 years (n=10), 7–10 years (n=13), 11–14 years (n=13) and 15–18 years (n=14) by averaging spatially normalized FDG-PET images of individual controls belonging to each of the five age-ranges. Secondly, for individual patients, FDG-PET image volumes were spatially normalized into standard stereotactic space using age-matched FDG-PET templates. The experimental parameters of

this spatial normalization process have been described previously [Kumar et al., 2010]. Thirdly, the spatially normalized images of individual patients were compared at voxel level to the age-matched pseudo-normal controls using a two-sample t-test, with age as a covariate, with an SPM t-score map as the result. For each voxel, the significance of two conditions, patient < controls (hypometabolism), and patient > controls (hypermetabolism), were tested on the SPM t-score map to determine if the voxel belongs to either hypo-or hypermetabolic region at the given thresholds of statistical significance and cluster extent (> 50 voxels) [Kumar et al., 2010].

All significant hypo-/hyper-metabolic clusters were overlaid on the 3D cortical surface generated by FreeSurfer scripts (http://surfer.nmr.mgh.harvard.edu) from the high-resolution T1 image. The SPM-defined significant regions were transformed into native FDG-PET image space by applying the inverse of spatial deformation obtained between the subject's FDG image and age-matched template. An affine linear transformation was performed to co-register PET and T1 MR images. The resulting transformation was applied to co-register the SPM-defined abnormal metabolic region onto the high resolution T1 image including the 3D cortical surface. **Finally, SPM-t score values of the co-registered metabolic region intersected at the coordinates of individual vertices of 3D cortical surface were sampled for spatial comparison with adjacent ECoG localization of epileptic electrodes. It should be noted that the sampled t-scores are defined only on 3D cortical surface not in deep structures and also do not include the metabolic abnormalities that are not near 3D cortical surface**.

For PET/ECoG comparisons, MRI-based 3D cortical surfaces were created with the location of electrodes directly defined on the cortical surface, as described previously [Alkonyi et al, 2009; Asano et al., 2009]. The spatial accuracy of electrode display on the three-dimensional brain surface image was visually confirmed by direct visualization of intraoperative pictures, which have been treated as the gold-standard to determine the co-registration accuracy [Wellmer et al., 2002; Dalal et al., 2008; Pieters et al., 2013]. Post-implant CT images were used, as needed, to confirm the co-registration accuracy on the medial and inferior surfaces of the cortex [Tao et al., 2009].

## Statistical analysis

To assess the detailed spatial relation between metabolic abnormalities and ECoG-defined SOZ, 3D SPM t-score surface maps of individual patients were thresholded at 10 different t-scores, i.e., ±2, ±2.5, ±3, ±3.5, and ±4.0 corresponding to SPM p-value = 0.03, 0.01, 0.005, 0.002, 0.0007, respectively ('+' and '−' correspond to hyper- and hypometabolism, respectively). For each of the t-score thresholds, the Euclidean distance of the electrode center from the closest edge of the metabolic cluster was calculated at five different distance ranges, i.e., ≤10mm (i.e, within one electrode distance corresponding to "overlap"), ≤15mm, ≤20 mm, ≤25 mm and ≤30 mm distance. For each of two discrete thresholds in t-score and distance, we determined both sensitivity and specificity of 3D surface map based on whether any of hypometabolic clusters obtained at the given t-score was located within the given distance from the nearest SOZ electrode. Likewise, we assessed the spatial relation between metabolic abnormalities and 'interictal spike zone'. We tested the performance of FDG PET

for both outcome measures (SOZ and interictal spike zone) in each patient individually and then averaged for the whole group, as well as in multiple subgroups based on focal vs. widespread SOZ, focal vs. widespread interictal spike zone, age (<4 years vs. >4 years of age), epilepsy duration (short vs. long, < 6 years vs. > 6 years), the presence of focal cortical dysplasia (FCD), and surgical outcome (recurrent seizures vs. seizure free 1 year after surgery). One-way ANOVA with age as a covariate was utilized to test significant group differences in sensitivity and specificity at $p < 0.05$.

In addition, the sensitivity and specificity of SPM-detected glucose metabolic abnormalities were evaluated on the lobar level. In this analysis, the lobar location of hypo- and hypermetabolic clusters was noted and compared to lobar locations of the SOZ (as indicated in Table 1) in the hemisphere included in the intracranial EEG monitoring (i.e., surgical hemisphere). Lobar co-localization of metabolic clusters and SOZ electrodes was defined as "true positive", metabolic cluster in a lobe with no SOZ was "false positive", SOZ in a lobe with no SPM-defined metabolic abnormality was considered "false negative", and a lobe with neither SOZ nor metabolic abnormality was "true negative".

## Results

### Demonstration of correspondence of SPM findings, visual PET abnormalities, and ECoG findings

First, we inspected how SPM-defined metabolic abnormalities correspond to visually detected PET abnormalities. Figure 1 presents representative examples of hypo/hyper-metabolic abnormalities obtained from 3D SPM t-score maps, which demonstrate good correspondence with hypo/hypermetabolic cortical areas displayed on 2D FDG-PET slices of interest, with $s_1/s_2$ demonstrating abnormal/normal metabolic pattern, respectively. Also, to demonstrate the feasibility of 3D SPM t-score visualization to detect significant metabolic changes corresponding to ECoG-defined SOZ, we present representative examples showing different degrees of spatial correspondence between ECoG and 3D SPM t-score surface maps of FDG-PET (Figure 2). The first examples show significant hypometablic clusters partially overlapped with ECoG-defined SOZ (Fig. 2A). Also, we found examples of significant hypermetabolic clusters partially overlapped with (or proximal to) 'interictal spiking zone' (Fig. 2B). In some cases, no metabolic abnormality was found despite the presence of extensive SOZ (Fig. 2C). Altogether, these comparisons demonstrated a complex relation between location/extent of SPM t-score surface maps and ECoG abnormalities; these were further analyzed quantitatively.

### Accuracy of 3D SPM t-score maps to detect ECoG-defined SOZ and interictal spiking in the whole group

Sensitivity and specificity of 3D SPM t-score maps to detect ECoG-defined SOZ (n=692) and 'interictal spiking zone' (n=1760) were assessed in the whole group (n=37, Fig. 3), where each measure was evaluated as a function of 10 discrete SPM t-score thresholds (±2.0, 2.5, 3.0, 3.5 and 4.0) and 5 discrete Euclidean distances between ECoG electrode coordinate and SPM t-score coordinate on 3D brain surface (≤10 mm, 15 mm, 20 mm, 25 mm, 30 mm). The sensitivity to detect SOZ by hypometabolic clusters was highest at the

threshold of t= −2 and linearly decreased up to the threshold of t= −4.0 (i.e., sensitivity gradually decreased from 0.30 to 0.09 within 10mm, 0.32–0.10 within 15mm, 0.34–0.10 within 20mm, 0.36–0.11 within 25mm and 0.39–0.12 within 30mm distance from SOZ electrodes, respectively). In the same range of t-thresholds (−2 to −4), the specificity to detect ECoG SOZ varied 0.88–0.98/0.85–0.97/0.83–0.96/0.81–0.96/0.79–0.95 within the same distance range (i.e., 10mm/15mm/20mm/25mm/30mm, respectively) of hypometabolic clusters from SOZ electrodes. In the same range of t-thresholds, the specificity to detect ECoG SOZ varied 0.88–0.98/0.85–0.97/0.83–0.96/0.81–0.96/0.79–0.95 within the distance range of hypometabolic clusters from SOZ electrodes, respectively.

Based on the presence of statistically significant linearity observed between sensitivity and t-threshold (e.g., ANOVA of a linear regression model: sensitivity = β·t-threshold+age where β is a fitting coefficient, $p < 0.008$ for all five distances), the middle t-threshold of t= −3.0 was selected as “reference t-threshold” for further comparison where the sensitivity of 0.18/0.20/0.22/0.23/0.25 and the specificity of 0.94/0.93/0.93/0.91/0.90 were observed to detect SOZ hypometabolic clusters within 10mm/15mm/20mm/25mm/30mm distance from SOZ electrodes, respectively. At the same reference t-threshold of t= 3.0 for hypermetabolism, we found much lower sensitivity with slightly higher specificity values to detect SOZ by hypermetabolic clusters (i.e., 0.02–0.04 and 0.98–0.94 for sensitivity and specificity within 10mm–30mm distance range from SOZ electrodes, respectively).

The sensitivity of hypometabolic clusters to detect ‘interictal spike zone’ at the reference threshold of t= −3.0 was lower than sensitivity for SOZ (i.e., 0.11/0.12/0.14/0.15/0.16 within 10mm/15mm/20mm/25mm/30mm distance from ECoG interictal spike electrodes, respectively). The specificity of hypometabolic clusters to detect ‘interictal spike zone’ was similar to specificity for SOZ (0.98/0.97/0.96/0.95/0.94 within 10mm/15mm/20mm/25mm/30mm distance from ‘interictal spiking zone’, respectively). The sensitivity of hypermetabolic clusters to detect ‘interictal spike zone’ was very low (varying 0.01–0.03 within 10mm–30mm distance range), while the specificity was similar to that of hypometabolic clusters (varying 0.97–0.93 within 10mm–30mm distance range from ‘interictal spike zone’).

### Percentage of patients showing overlap between ECoG-defined ictal and interictal abnormalities and SPM-defined metabolic abnormalities

Table 2 summarizes the percentages of patients who had at least one cluster of metabolic changes on (or near) ECoG-defined SOZ and ‘interictal spike zone’ assessed with two different criteria: (i) the threshold of SPM t-score map and (ii) the nearest distance between the outer boundary of SPM cluster and ECoG electrode. At the reference mid-threshold of t= −3.0, 55% of patients showed at least one cluster of hypometabolic abnormality overlapped with the SOZ, while 71% of patients showed at least one cluster of hypometabolic abnormality overlapped with ‘interictal spike zone’. In contrast, at the same threshold, only 13% and 21% of patients showed at least one cluster of hypermetabolic abnormality overlapped with SOZ and ‘interictal spike zone’, respectively.

### Accuracy of 3D SPM t-score maps to detect ECoG-defined SOZ and interictal spiking in subgroups

Based on histogram analyses in the number of SOZ (Fig. 4A) and interictal spiking electrodes (Fig. 5A), we have divided the patients into two subgroups: focal vs. widespread SOZ (i.e., less and greater than 20 electrodes involved) and focal vs. widespread 'interictal spiking zone' (i.e., less and greater than 37 electrodes involved). Compared with the widespread SOZ group at the reference threshold of t= −3.0, the focal SOZ group showed statistically similar sensitivity/specificity within 10 mm distance (sensitivity=0.22±0.06/0.08±0.03, p=0.14, specificity=0.95±0.02/0.93±0.02, p=0.77 for focal/widespread SOZ subgroup, Fig 4B). At the reference threshold of t= −3.0, sensitivity and specificity were similar in the focal vs. widespread 'interictal spike zones' (i.e., sensitivity=0.12±0.04/0.10±0.04, p=0.76, specificity=0.96±0.01/0.96±0.01, p=0.96 for focal/widespread interictal spike zone, Fig 5B).

In other subgroup analyses, in young children less than 4 years of age, the sensitivity of hypometabolic area to detect ECoG-defined SOZ was 0.12±0.06 for overlap (i.e., within 10mm distance) and 0.20±0.08 within 30 mm distance, which was only slightly lower than in the children older than 4 years of age (0.20±0.06, p=0.20 and 0.27±0.07, p=0.16, respectively). Both subgroups showed similar specificity values for both overlap and 30 mm distance (up to about 0.93±0.02 for overlap in young children). There was no statistical difference between shorter and longer epilepsy duration groups (p-value=0.19 for overlap). Also, no statistical difference was found between FCD (n=8 children) and non-FCD subgroups (n=29) where p-value was 0.63 for comparison of overlap. Finally, children with post-operative recurrent seizures showed similar sensitivity (0.23±0.06 vs. 0.31±0.10, p=0.47 for 30 mm distance) and slightly higher specificity (0.92±0.01 vs. 0.85±0.05, p =0.07 for 30 mm distance) than the children with seizure-free surgical outcome.

In the present study, all subgroup comparisons were insignificant in the corresponding ANOVAs as reported above (i.e., uncorrected $p<0.05$). Thus, corrections of those significances were not performed for multiple comparisons. This had no effect on the results considering that none of these subgroup comparisons were significant when using an uncorrected $p<0.05$.

### Accuracy of FDG-PET SPM analysis to detect lobe(s) of SOZ

The lobar locations of glucose metabolic abnormalities using SPM analysis at our reference t-threshold (SPM t-score = ± 3.0) and extent threshold of > 50 in the affected (surgical) hemisphere are reported in Table 1. At least one cluster of metabolic abnormality was found in 34/37 (92%) patients for hypometabolism and in 25/37 (67%) for hypermetabolism; only one patient (#20) had completely negative PET results at this threshold. In the 25 patients showing an area of increased metabolism on SPM, 17 (68%) showed frequent (>10 per minute; n=9) or rare/occasional (<10 per minute; n=8) interictal epileptiform activity on scalp EEG during the FDG uptake period. Five additional patients with interictal epileptiform activity showed no hypermetabolism. Hypometabolic clusters had a sensitivity of 74.6% and a specificity of 64.2% to detect the lobe of ECoG-defined SOZ. Meanwhile, a much lower lobar sensitivity of 34.3% and somewhat higher lobar specificity of 69.1% were

found for hypermetabolic clusters. The values were similar for a young subgroup including 10 children below 4 years of age (sensitivity of 79%/29%, specificity of 56%/81% for hypo-/hypermetabolic cluster).

## Discussion

The present study demonstrates that SPM-based brain surface analysis, using age-matched pseudo-control groups (1–18 years), can be applied to detect glucose metabolic abnormalities objectively on (or near) SOZ identified by ECoG in pediatric epilepsy in children above 1 year of age. We have shown that lobar accuracy of detection of the SOZ is similar to previously reported lobar accuracies in older pediatric and young adult groups [Lee et al., 2005; Kumar et al., 2010; Archambaud et al., 2013; vant' Klooster et al., 2014]. In addition, by directly measuring the nearest Euclidean distance between ECoG-defined SOZ and SPM metabolic clusters on the actual 3D brain surface of individual patients, we found that 1) large portions of the hypometabolic abnormalities are located outside the SOZ, often at 30mm distance or beyond; 2) the hypometabolic abnormality provided slightly higher sensitivity to overlap focal SOZ than widespread SOZ; 3) hypermetabolic clusters were detected in 2/3 of the cases and were often associated with interictal epileptiform activity during FDG uptake; however, these hypermetabolic abnormalities were also observed mostly outside the ECoG-defined SOZ or 'interictal spike zone'. 4) Performance of hypometabolic abnormality to detect ECoG-defined SOZ was comparable in young patients as compared to the older subgroup, and did not differ in those with seizure-free vs. not seizure-free outcome.

To the best of our knowledge, the present study is the first to quantitatively assess Euclidian distances between SPM-defined FDG-PET glucose metabolic abnormalities and ECoG-defined epilepsy biomarkers such as SOZ and 'interictal spike zone'. Although several previous studies utilized voxel-wise SPM analysis to objectively detect metabolic abnormalities in children with intractable epilepsy, none of those studies have reported how closely and accurately the SPM-defined cluster can detect ECoG-defined SOZ. Specifically, to define PET accuracy, the partial or total overlap of the hypometabolic region with the SOZ had been determined on either lobar basis or gyral level in previous studies [Kumar et al., 2010; Archambaud et al., 2013; vant' Klooster et al., 2014]. This approximation of spatial correspondence inevitably resulted in variable performance of SPM analysis across the literature (e.g., sensitivity/specificity= 0.86/0.77 [Kumar et al., 2010], 0.79/0.97 [Archambaud et al., 2013], 0.35/0.90 [vant' Klooster et al., 2014]).

Two previous studies from our group have used an asymmetry-based approach to compare the performance of FDG-PET against ECoG-defined SOZ in small pediatric groups with epilepsy surgery [Juhász et al., 2000; Alkonyi et al., 2009]. A recent study, using stereo-EEG, also found a poor correlation between hypometabolic cortex and iHFOs in patients with extratemporal seizure foci [Lamarche et al., 2016]. Despite the different PET analytic approaches, both those previous and our current results demonstrated a mismatch between hypometabolic and epileptogenic cortex, which appears to be present regardless of age or epilepsy duration. Indeed, the majority of hypometabolic (and also hypermetabolic) regions do not appear to be involved in seizure generation. This is consistent with the notion that

decreased cortical glucose metabolism may reflect neuronal loss leading to a decrease of synaptic activity in the epileptic brain without actual epileptogenicity [Szelies et al., 1983; Lippa et al., 1993]. In fact, seizures often originate from mildly hypometabolic areas adjacent to the cortical lesions such as tubers, rather than within severely hypometabolic lesions [Major et al., 2009]. Similarly, SOZ electrodes were detected >1.5 cm beyond tumor margins in low-grade brain tumors [Mittal et al., 2016]. Thus, the selection of an optimal SPM t-threshold, performed in the present study, is a critical step that can affect the overall accuracy of SPM-detected metabolic abnormalities for prediction of SOZ.

Our data also demonstrate that SOZ and 'interictal spike zone' are often located outside but in proximity to hypometabolic cortex in the same lobe leading to significantly higher accuracy when lobar localization is applied. This is consistent not only with our previous PET/EEG studies [Juhász et al., 2000; Alkonyi et al., 2009] but also with EEG-triggered fMRI data demonstrating BOLD signals at the border of hypometabolic regions rather than in the center of hypometabolism [Donaire et al., 2013]. Altogether, these observations support the notion that decreased neocortical metabolism may partly represent an inhibitory area with a higher threshold for seizure initiation (consistent with the classic concept of "surround inhibition" [Prince and Wilder, 1967]. Thus, the clinical utility of FDG PET in guiding subdural electrode placement in neocortical epilepsy could be enhanced by extending grid coverage to 3 cm beyond hypometabolic cortex, when feasible. In fact, the current study could find that about 53% and 68% of children with intractable epilepsy show at least one SOZ and 'interictal spike zone' within this 3 cm margin near SPM hypometabolic clusters measured at t= −3.5 (Table 2). Importantly, FDG-PET may perform best in this regard if scalp EEG suggests a more focal (rather than widespread, multilobar) onset; in such cases, more restricted grid coverage on/around the hypometabolic area may be sufficient.

To obtain an accurate, objective, and detailed comparison of FDG-PET and ECoG abnormalities, the present study rendered both SPM-defined metabolic abnormalities and ECoG electrode locations to the same native 3D brain surface and directly measured the physical distance between the coordinate of SPM metabolic vertex and epileptic electrode vertex as a function of variable statistical thresholds. This approach allowed us to accurately assess the spatial relation between metabolic and electrophysiological mismatch at different degrees of statistical inference. Two previous pediatric studies with SPM analysis [Kumar et al., 2010; Archambaud et al., 2013] used a p-value < 0.001 as a statistical cut-off threshold to find SOZ in lobar classification leading to sensitivity of 0.79 to 0.86 and specificity of 0.77 to 0.97. Another study including children and adults with non-lesional epilepsy used the same SPM threshold and found concordance between FDG-PET abnormalities and SOZ in only 44% of the cases [Lee et al., 2005]. However, none of these studies utilized pediatric templates and pediatric control data younger than 5 years of age for SPM analysis, and the reported values were limited to lobar correspondence without considering the actual distance from ECoG-defined SOZ. The reported values were limited to lobar correspondence without considering the actual distance from ECoG-defined SOZ. Using a similar statistical threshold, we found a comparable (albeit slightly lower) lobar accuracy in the present study (i.e., sensitivity of 74.6% and a specificity of 64.2% to detect the lobe of ECoG-defined SOZ by hypometabolism), even though our patient group had a wide age range including very

young subjects. This sensitivity/specificity values were substantially higher than expected by chance: a random permutation test to match the lobar SOZ and hypometabolic lobes showed that 53.3% sensitivity and 46.6% specificity could be expected by chance, considering the extent of electrophysiologic and metabolic abnormalities in this group.

Unlike most previous studies analyzing the spatial relation between glucose metabolic abnormalities and intracranial EEG findings, our study analyzed not only hypo- but also hypermetabolic abnormalities. Interestingly, hypermetabolic clusters in the affected hemisphere were surprisingly common (present in 2/3 of our cases), and were often associated with interictal spiking on EEG recorded during PET **(17/25)**. However, frequent spiking was only observed in 9 of 25 cases (36%), and the hypermetabolic clusters were relatively rarely located in close vicinity to the SOZ or even ‘interictal spike zone’ on ECoG. In addition, the lobar sensitivity of hypermetabolic clusters to detect SOZ was modest (34%) at the threshold of SPM t-score of 3.0. At this threshold we could find only 21% and 37% of our patients showing at least one hypermetabolic cluster within 3 cm margin from SOZ and ‘interictal spike zone’, respectively. Thus, while hypermetabolic clusters may reflect increased metabolism due to ongoing interictal spiking during the FDG uptake period, they appear to provide only a modest contribution to localization of the ECoG-defined SOZ.

The present study found that accuracy of SPM surface analysis was not related to 1-year surgical outcome. This is consistent with our previous study in children with neocortical epilepsy showing that extent of resected hypometabolic cortex did not affect surgical outcome [Juhász et al., 2001]. Both results are consistent with the notion that the bulk of hypometabolic cortex is non-epileptic, and, therefore, extent of cortical glucose metabolic abnormalities can only assist the design of the intracranial electrode placement on the lobar level without guiding the resection itself.

In conclusion, SPM surface analysis using an age-matched pseudo-control group can be applied as an objective analytic method to identify cortical regions with hypo- and hypermetabolism **on** PET in children of a wide age-range. This approach may allow the FDG-PET localization of epileptic foci with a good accuracy on the lobar level, but has a low sensitivity to delineate the exact SOZ within the lobes. Considering that the extent of intracranial electrode coverage is inevitably limited, localization information from other modalities including scalp EEG, seizure semiology, MRI, SPECT and/or MEG should be considered in patients with large hypometabolic cortex, to increase the chance of sufficient coverage of the epileptogenic zone to be resected. Usage of both subdural and depth electrodes may optimize the spatial sampling in subsets of patients with drug-resistant focal epilepsy. FDG-PET may provide a reasonable estimate of epileptic cortex in cases with relatively focal SOZ.

## Acknowledgments

Special thanks to Thomas Mangner, Ph.D. for the reliable radiosynthesis of FDG, as well as Galina Rabkin, CNMT, Angela Wigeluk, CNMT, Carole Klapko, CNMT and Andrew Masqueda CNMT for their expert technical assistance in performing the PET studies. We are also grateful to the whole staff of the Division of Electroneurodiagnostics at Children’s Hospital of Michigan, Wayne State University, for their assistance in performing the extraoperative ECoG studies. This study was funded by a grant from National Institute of Neurological Disorders and Stroke (R01-NS089659 to JJ).

## References


Alkonyi B, Juhász C, Muzik O, Asano E, Saporta A, Shah A, Chugani HT. Quantitative brain surface mapping of an electrophysiologic/metabolic mismatch in human neocortical epilepsy. Epilepsy Res. 2009; 87:77–87. [PubMed: 19734012]

Archambaud F, Bouilleret V, Hertz-Pannier L, Chaumet-Riffaud P, Rodrigo S, Dulac O, Chassoux F, Chiron C. Optimizing statistical parametric mapping analysis of 18F-FDG PET in children. EJNMMI Res. 2013; 3:2.doi: 10.1186/2191-219X-3-2 [PubMed: 23289862]

Asano E, Juhasz C, Shah A, Sood S, Chugani HT. Role of subdural electrocorticography in prediction of long-term seizure outcome in epilepsy surgery. Brain. 2009; 132:1038–47. [PubMed: 19286694]

Asano E, Brown EC, Juhász C. How to establish causality in epilepsy surgery. Brain Dev. 2013; 35:706–20. [PubMed: 23684007]

Canolty RT, Edwards E, Dalal SS, Soltani M, Nagarajan SS, Kirsch HE, Berger MS, Barbaro NM, Knight RT. High gamma power is phase-locked to theta oscillations in human neocortex. Science. 2006; 313:1626–8. [PubMed: 16973878]

Chugani HT, Asano E, Juhász C, Kumar A, Kupsky WJ, Sood S. Subtotal hemispherectomy in children with intractable focal epilepsy. Epilepsia. 2014; 55:1926–33. [PubMed: 25366422]

Chugani HT, Phelps ME, Mazziotta JC. Positron emission tomography study of human brain functional development. Ann Neurol. 1987; 22:487–97. [PubMed: 3501693]

Chugani HT, Phelps ME. Maturational changes in cerebral function in infants determined by 18FDG positron emission tomography. Science. 1986; 231:840–3. [PubMed: 3945811]

Crone NE, Boatman D, Gordon B, Hao L. Induced electrocorticographic gamma activity during auditory perception. Clin Neurophysiol. 2001; 112:565–82. [PubMed: 11275528]

da Silva EA, Chugani DC, Muzik O, Chugani HT. Identification of frontal lobe epileptic foci in children using positron emission tomography. Epilepsia. 1997; 38:1198–208. [PubMed: 9579921]

Dalal SS, Edwards E, Kirsch HE, Barbaro NM, Knight RT, Nagarajan SS. Localization of neurosurgically implanted electrodes via photograph-MRI-radiograph coregistration. J Neurosci Methods. 2008; 174:106–15. [PubMed: 18657573]

Donaire A, Capdevila A, Carreno M, Setoain X, Rumia J, Aparicio J, Campistol J, Padilla N, Sanmarti F, Vernet O, Pintor L, Boget T, Ortells J, Bargallo N. Identification the cortical substrates of interictal epileptiform activity in patients with extratemporal epilepsy: An EEG-fMRI sequential analysis and FDG-PET study. Epilepsia. 2013; 54:678–90. [PubMed: 23362864]

Fischl B, Liu A, Dale AM. Automated manifold surgery: constructing geometrically accurate and topologically correct models of the human cerebral cortex. IEEE Trans Med Imaging. 2001; 20:70–80. [PubMed: 11293693]

Fischl B, Salat DH, van der Kouwe AJ, Makris N, Segonne F, Quinn BT, Dale AM. Sequence-independent segmentation of magnetic resonance images. Neuroimage. 2004; 23(Suppl 1):S69–84. [PubMed: 15501102]

Foster BL, Kaveh A, Dastjerdi M, Miller KJ, Parvizi J. Human retrosplenial cortex displays transient theta phase locking with medial temporal cortex prior to activation during autobiographical memory retrieval. J Neurosci. 2013; 33:10439–46. [PubMed: 23785155]

Friston KJ, Poline JB, Homes AP, Frith C, Frackowiak RSJ. A multivariate analysis of PET activation studies. Hum Brain Mapp. 1996; 4:140–51. [PubMed: 20408193]

Fujiwara H, Greiner HM, Lee KH, Holland-Bouley KD, Seo JH, Arthur T, Mangano FT, Leach JL, Rose DF. Resection of ictal high-frequency oscillations leads to favorable surgical outcome in pediatric epilepsy. Epilepsia. 2012; 53:1607–17. [PubMed: 22905734]

Hader WJ, Mackay M, Otsubo H, Chitoku S, Weiss S, Becker L, Snead OC 3rd, Rutka JT. Cortical dysplastic lesions in children with intractable epilepsy: role of complete resection. J Neurosurg. 2004; 100:110–7. [PubMed: 14758938]

Hong KS, Lee SK, Kim JY, Lee DS, Chung CK. Pre-surgical evaluation and surgical outcome of 41 patients with non-lesional neocortical epilepsy. Seizure. 2002; 1:184–92.

Jayakar P, Gaillard WD, Tripathi M, Libenson MH, Mathern GW, Cross JH, Task Force for Paediatric Epilepsy Surgery, Commission for Paediatrics, and the Diagnostic Commission of the International

League Against Epilepsy. Diagnostic test utilization in evaluation for resective epilepsy surgery in children. Epilepsia. 2014; 55:507–18. [PubMed: 24512473]

Juhász C, Chugani DC, Muzik O, Shah A, Asano E, Mangner TJ, Chakraborty PK, Sood S, Chugani HT. Alpha-methyl-L-tryptophan PET detects epileptogenic cortex in children with intractable epilepsy. Neurology. 2003; 60:960–8. [PubMed: 12654960]

Juhász C, Chugani DC, Muzik O, Watson C, Shah J, Shah A, Chugani HT. Is epileptogenic cortex truly hypometabolic on interictal positron emission tomography? Ann Neurol. 2000; 48:88–96. [PubMed: 10894220]

Juhász C, Chugani DC, Muzik O, Shah A, Shah J, Watson C, Canady A, Chugani HT. Relationship of flumazenil and glucose PET abnormalities to neocortical epilepsy surgery outcome. Neurology. 2001; 56:1650–8. [PubMed: 11425929]

Juhász C. The impact of positron emission tomography imaging on the clinical management of patients with epilepsy. Expert Rev Neurother. 2012; 12:719–32. [PubMed: 22650174]

Kim YK, Lee DS, Lee SK, Chung CK, Chung JK, Lee MC. FDG PET in localization of frontal lobe epilepsy: comparison of visual and SPM analysis. J Nucl Med. 2002; 43:1167–74. [PubMed: 12215554]

Kim YK, Lee DS, Lee SK, Chung CK, Chang KH, Choy JK, Lee MC. Differential features of metabolic abnormalities between medial and lateral temporal lobe epilepsy: quantitative analysis of 18F-FDG PET using SPM. J Nucl Med. 2003; 44:1006–12. [PubMed: 12843213]

Kumar A, Juhasz C, Asano E, Sood S, Muzik O, Chugani HT. Objective detection of epileptic foci by 18F-FDG PET in children undergoing epilepsy surgery. J Nucl Med. 2010; 51:1901–7. [PubMed: 21078805]

Lamarche F, Job AS, Deman P, Bhattacharjee M, Hoffmann D, Gallazzini-Crépin C, Bouvard S, Minotti L, Kahane P, David O. Correlation of FDG-PET hypometabolism and SEEG epileptogenicity mapping in patients with drug-resistant focal epilepsy. Epilepsia. 2016; 57:2045–55. [PubMed: 27861778]

Lee SK, Lee SY, Kim KK, Hong KS, Lee DS, Chung CK. Surgical outcome and prognostic factors of cryptogenic neocortical epilepsy. Ann Neurol. 2015; 58:525–32.

Lippa CF, Pearson D, Smith TW. Cortical tubers demonstrate reduced immunoreactivity for synapsin I. Acta Neuropathol. 1993; 85:449–51. [PubMed: 8480517]

Major P, Rakowski S, Simon MV, Cheng ML, Eskandar E, Baron J, Leeman BA, Frosch MP, Thiele EA. Are cortical tubers epileptogenic? *Evidence from electrocorticography*. Epilepsia. 2009; 50:147–54. [PubMed: 19125835]

Mittal S, Barkmeier D, Hua J, Pai DS, Fuerst D, Basha M, Loeb JA, Shah AK. Intracranial EEG analysis in tumor-related epilepsy: Evidence of distant epileptic abnormalities. Clin Neurophysiol. 2016; 127:238–44. [PubMed: 26493495]

Muzik O, Chugani DC, Juhasz C, Shen C, Chugani HT. Statistical parametric mapping: assessment of application in children. Neuroimage. 2000; 12:538–49. [PubMed: 11034861]

Nagasawa T, Juhász C, Rothermel R, Hoechstetter K, Sood S, Asano E. Spontaneous and visually driven high-frequency oscillations in the occipital cortex: intracranial recording in epileptic patients. Hum Brain Mapp. 2012; 33:569–83. [PubMed: 21432945]

Palmini A, Gambardella A, Andermann F, Dubeau F, da Costa JC, Olivier A, Tampieri D, Gloor P, Quesney F, Andermann E, et al. Intrinsic epileptogenicity of human dysplastic cortex as suggested by corticography and surgical results. Ann Neurol. 1995; 37:476–87. [PubMed: 7717684]

Pieters TA, Conner CR, Tandon N. Recursive grid partitioning on a cortical surface model: an optimized technique for the localization of implanted subdural electrodes. J Neurosurg. 2013; 118:1086–97. [PubMed: 23495883]

Price DA, Wilder BJ. Control mechanisms in cortical epileptogenic foci. “Surround” inhibition. Arch Neurol. 1967; 16:194–202. [PubMed: 6018049]

Rosenow F, Lüders H. Presurgical evaluation of epilepsy. Brain. 2001; 124:1683–700. [PubMed: 11522572]

Sakuraba R, Iwasaki M, Okumura E, Jin K, Kakisaka Y, Kato K, Tominaga T, Nakasato N. High frequency oscillations are less frequent but more specific to epileptogenicity during rapid eye movement sleep. Clin Neurophysiol. 2016; 127:179–86. [PubMed: 26073183]

Stanescu L, Ishak GE, Khanna PC, Biyyam DR, Shaw DW, Parisi MT. FDG PET of the brain in pediatric patients: imaging spectrum with MR imaging correlation. Radiographics. 2013; 33:1279–303. [PubMed: 24025925]

Szelies B, Herholz K, Heiss WD, Rackl A, Pawlik G, Wagner R, Ilsen HW, Wienhard K. Hypometabolic cortical lesions in tuberous sclerosis with epilepsy: demonstrated by positron emission tomography. J Comput Assist Tomogr. 1983; 7:946–53. [PubMed: 6415136]

Tao JX, Hawes-Ebersole S, Baldwin M, Shah S, Erickson SK, Ebersole JS. The accuracy and reliability of 3D CT/MRI co-registration in planning epilepsy surgery. Clin Neurophysiol. 2009; 120:748–53. [PubMed: 19264546]

vant' Klooster MA, Huiskamp G, Zijlmans M, Debets RM, Comans EF, Bouvard S, Ryvlin P, Leijten FS. Can we increase the yield of FDG-PET in the preoperative work-up for epilepsy surgery? Epilepsy Res. 2014; 108:1095–105. [PubMed: 24893829]

Weiss SA, Lemesiou A, Connors R, Banks GP, McKhann GM, Goodman RR, Zhao B, Filippi CG, Nowell M, Rodionov R, Diehl B, McEvoy AW, Walker MC, Trevelyan AJ, Bateman LM, Emerson RG, Schevon CA. Seizure localization using ictal phase-locked high gamma: A retrospective surgical outcome study. Neurology. 2015; 84:2320–8. [PubMed: 25972493]

Wellmer J, von Oertzen J, Schaller C, Urbach H, König R, Widman G, Van Roost D, Elger CE. Digital photography and 3D MRI-based multimodal imaging for individualized planning of resective neocortical epilepsy surgery. Epilepsia. 2002; 43:1543–50. [PubMed: 12460257]

Widdess-Walsh P, Jeha L, Nair D, Kotagal P, Bingaman W, Najm I. Subdural electrode analysis in focal cortical dysplasia: predictors of surgical outcome. Neurology. 2007; 69:660–7. [PubMed: 17698787]

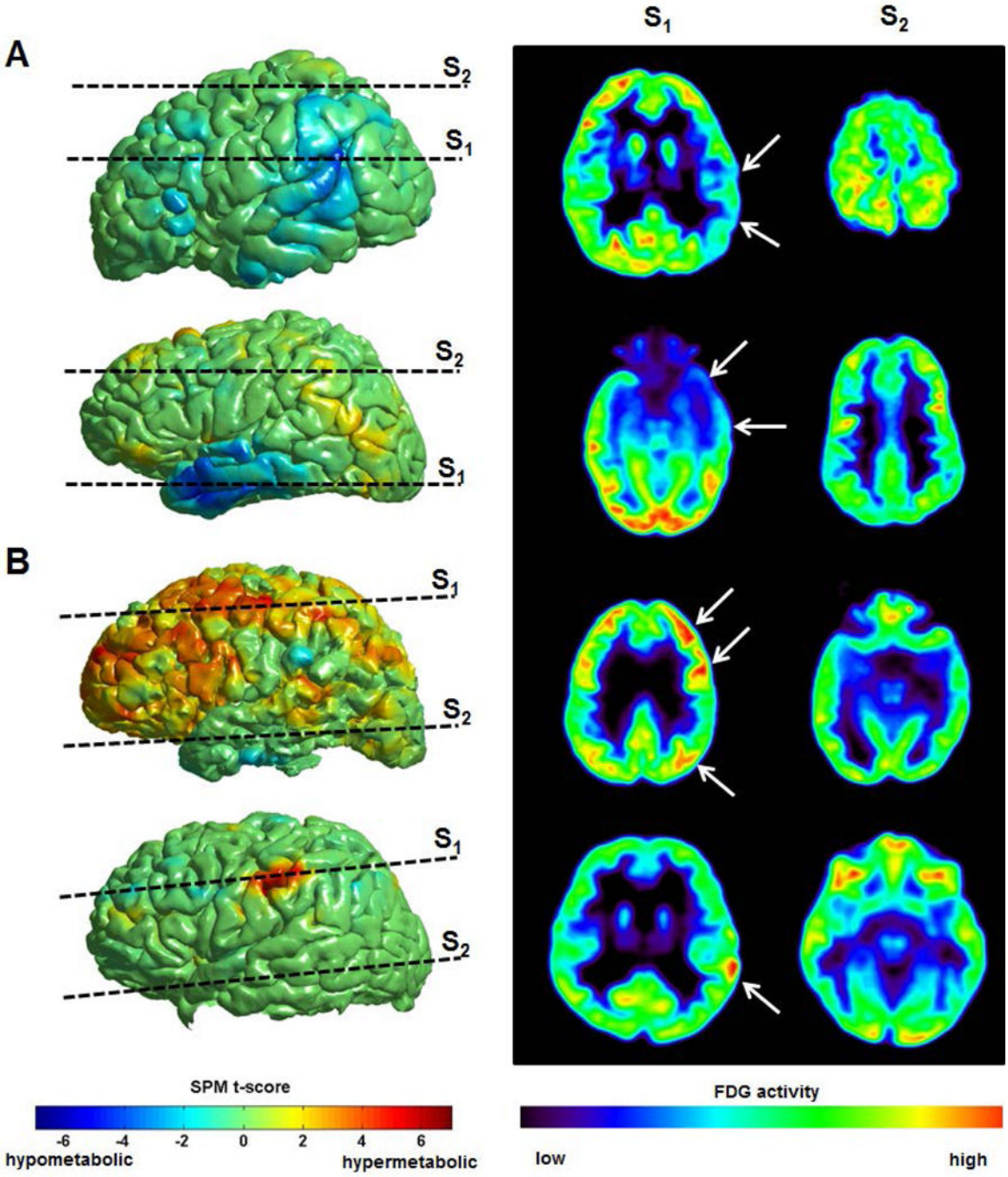


**Figure 1.**

Representative examples of 3D visualization maps which render SPM t-scores on FreeSurfer-driven pial surfaces (left column), and corresponding 2D FDG PET slices of interest, $s_1/s_2$ levels demonstrating abnormal/normal metabolic pattern, respectively (right column). (**A**) Hypometabolic pattern in two patients: each of two 3D maps shows a significant hypometabolic cluster detected in $s_1$ level of each individual patient, in the parietal lobe (top) and inferior temporal lobe (bottom), which are matched with low FDG activity in parietal cortex (top arrows) and inferior temporal cortex (bottom arrows) on

individual PET slices, $s_1$. Meanwhile, no additional hypometabolic cluster is depicted on a slice showing normal glucose metabolism, $s_2$ of either 3D surface map or 2D FDG PET. (**B**) Hypermetabolic pattern in two patients: each of two 3D maps shows a significant hypermetabolic cluster detected in $s_1$ level of individual patients, in the superior frontal and parietal lobe (top) and anterior parietal lobe (bottom) matched with high FDG activity seen in the superior frontal and parietal cortex (top arrows) and anterior parietal cortex (bottom arrow) on individual PET slices, $s_1$. Meanwhile, no additional hypermetabolic cluster is depicted on an axial slice through the temporal lobe, $s_2$ of either 3D surface map or 2D FDG PET. Please note that some metabolic asymmetries seen on the native, axial PET images occur outside the SPM-detected clusters (as seen in the left occipital cortex on the top images). These may represent physiologic asymmetries or mild metabolic abnormalities not detected by SPM.

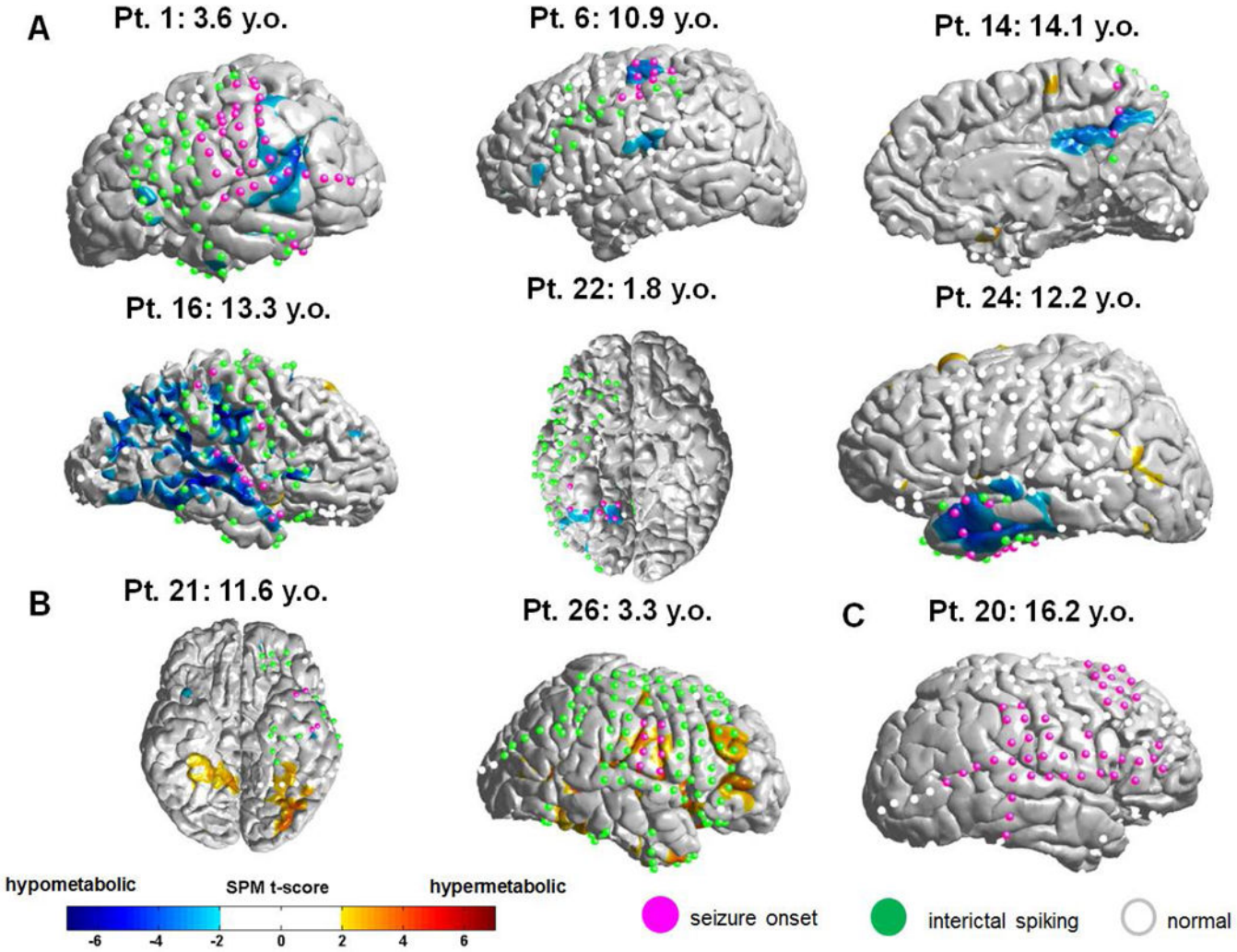


**Figure 2.**

Representative examples of spatial correspondence between ECoG and 3D SPM t-score surface maps of FDG-PET. (**A**) Examples of hypometablic clusters in six patients partially overlapped with ECoG-defined epileptogenic area, electrodes of seizure onset (magenta-colored circles). (**B**) Examples of hypermetabolic clusters partially overlapped with (or near) ECoG-defined interictal spike zone (green-colored circles). (**C**) Example of no metabolic abnormality in extensive epileptogenic area indicated by electrodes of seizure onset (magenta-colored circles).

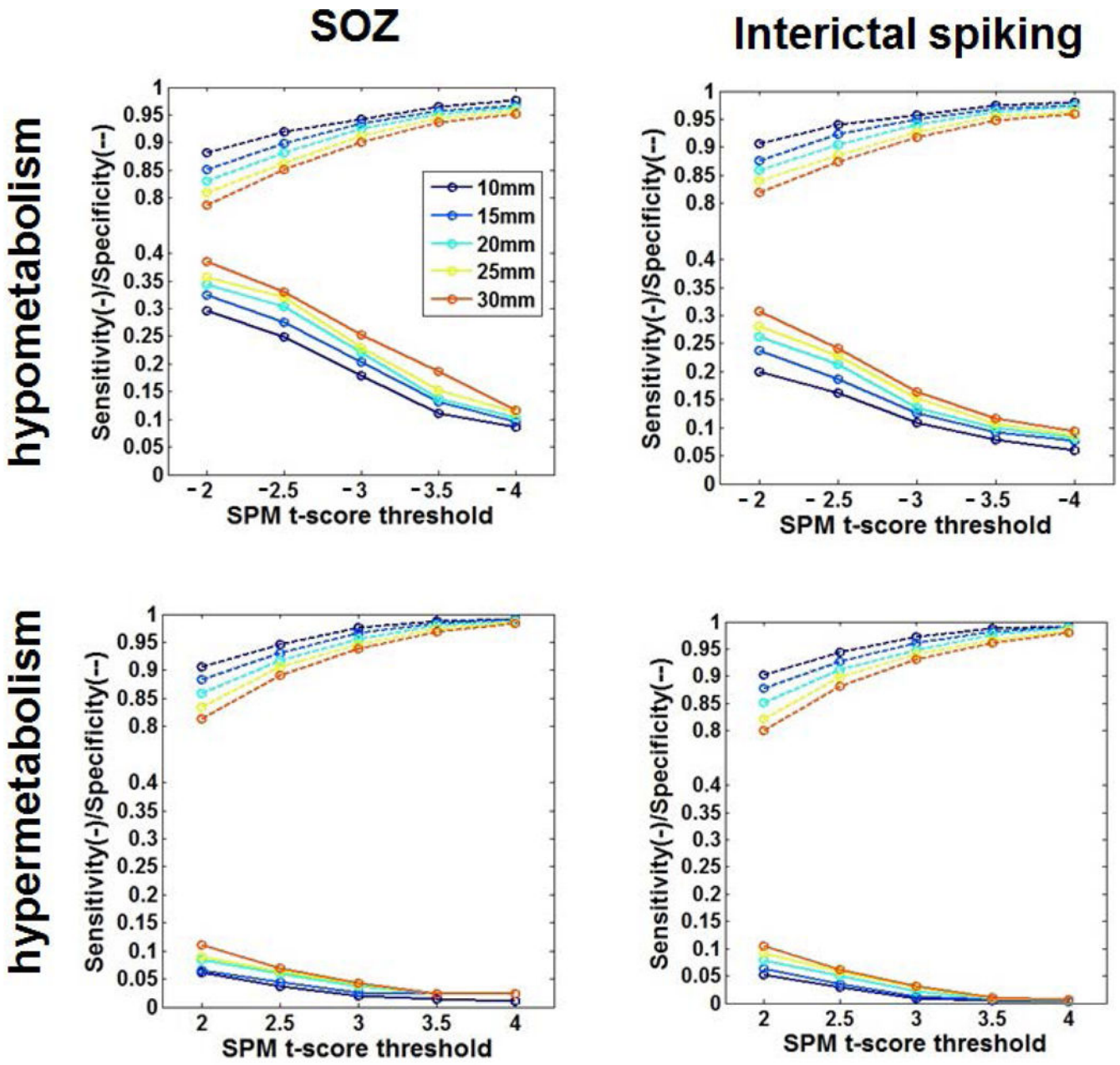


**Figure 3.**

Average sensitivity and specificity obtained from the whole group (n=37), hypometabolism (top) and hypermetabolism (bottom) of 3D SPM t-score surface map to detect ECoG-defined seizure onset zone (SOZ, left) and interictal spike zone (right). In each plot, sensitivity (solid lines) and specificity (dotted lines) of individual patient were assessed by two variables, SPM t-score threshold and Euclidean distance between ECoG electrode coordinate and SPM t-score coordinate in 3D pial surface and averaged in the whole group. Total numbers of ECoG electrodes were 692 and 1760 for SOZ and interictal spike zone, respectively.

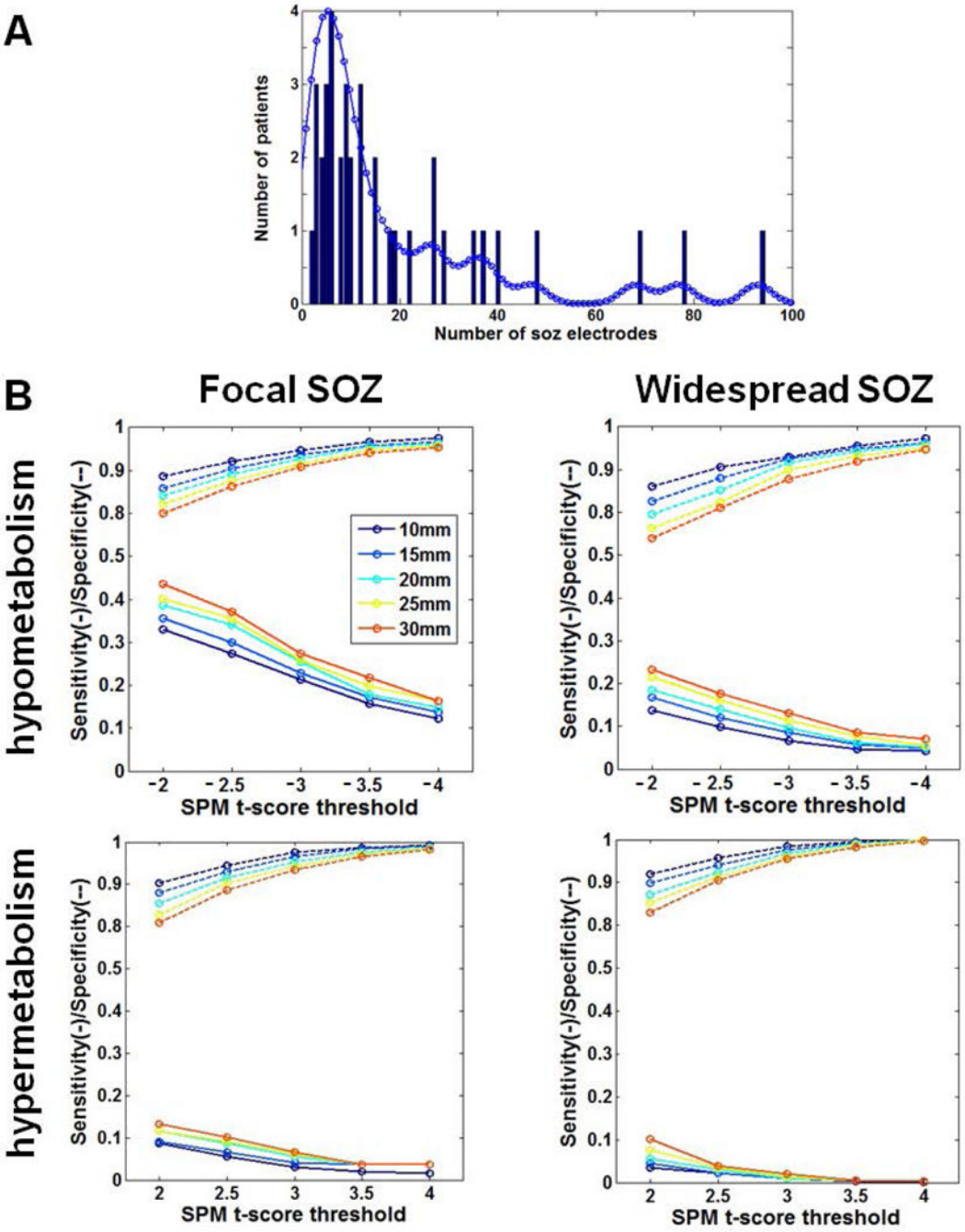


**Figure 4.**

Results of subgroup analysis: focal seizure onset zone (SOZ) vs. widespread seizure onset zone (SOZ). (**A**) A histogram of all patients (n=37) was obtained as the function of SOZ electrode number. The first valley of the fitted curve was observed at 20. This threshold was then applied to make two subgroups, focal SOZ (n=27) and widespread SOZ (n=10). (**B**) Average sensitivity and specificity obtained from each subgroup, hypometabolism (top) and hypermetabolism (bottom) of 3D SPM t-score map to detect ECoG-defined seizure onset zone (SOZ) in focal SOZ group (left) and widespread SOZ group (rights). In each plot,

sensitivity (solid lines) and specificity (dotted line) were assessed by two variables, SPM t-score threshold and Euclidean distance between ECoG electrode coordinate and SPM t-score coordinate in 3D cortical surface where ≤10 mm is defined as overlap. Total numbers of SOZ electrodes were 197 and 495 for focal and widespread SOZ subgroups, respectively.

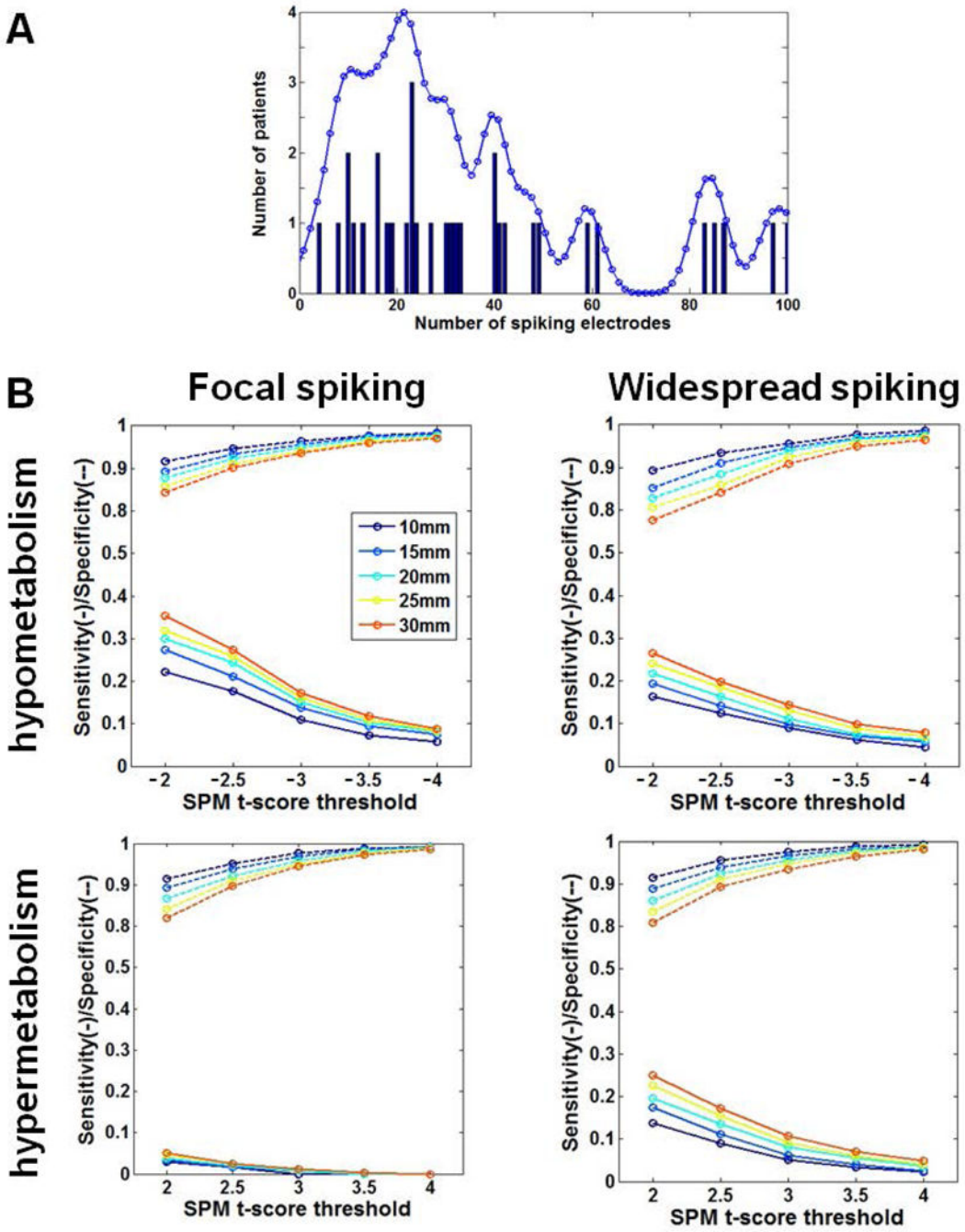


**Figure 5.**

Results of subgroup analysis: focal spiking vs. widespread spiking. (**A**) A histogram of all patients (n=37) was obtained as the function of interictal spiking electrode number. The first valley of the fitted curve was observed at 37. This threshold was then applied to make two subgroups, focal spiking (n=20) and widespread spiking (n=17). (**B**) Sensitivity and specificity of 3D SPM t-score maps, hypometabolism (top) and hypermetabolism (bottom) to detect ECoG-defined spiking in focal spiking group (left) and widespread spiking group (right). In each plot, sensitivity (solid lines) and specificity (dotted lines) were assessed by

two variables, SPM t-score threshold and Euclidean distance between ECoG electrode coordinate and SPM t-score coordinate in 3D cortical surface where ≤10 mm is defined as overlap. Total numbers of interictal spiking electrodes were 373 and 1387 for focal and widespread spiking subgroups, respectively.

**Table 1**

Clinical information, lobar locations of SPM-defined metabolic abnormalities and ECoG-defined seizure onset zone in the affected hemisphere.

| Pt. No. | Age (years) | Gender | Epilepsy duration (years) | Surgery side | ECoG Onset lobe(s) | SPM hypo | SPM hyper | Histology | Seizure Free |
|---|---|---|---|---|---|---|---|---|---|
| 1 | 3.6 | F | 3.3 | L | tpo | ftp | none | Gliosis | No |
| 2 | 10.6 | F | 8.3 | R | p | tp | none | Gliosis | Yes |
| 3 | 18.7 | F | 6.9 | R | ftp | ft | fp | Gliosis | Yes |
| 4 | 2.7 | M | 0.3 | L | f | fp | none | FCD | Yes |
| 5 | 9.1 | F | 1.8 | L | t | ft | none | Gliosis | Yes |
| 6 | 10.9 | F | 11 | L | fp | fp | f | TSC,gliosis | Yes |
| 7 | 11.2 | F | 8.3 | L | t | t | ftp | Gliosis | Yes |
| 8 | 7.7 | M | 4.8 | R | to | fp | fo | FCD | Yes |
| 9 | 11.6 | F | 11.6 | L | t | t | p | GG | Yes |
| 10 | 6.4 | F | 5.4 | L | t | t | none | Gliosis | Yes |
| 11 | 12.5 | F | 0.6 | L | p | tpo | f | OG | No |
| 12 | 14.3 | F | 8.5 | L | t | ft | ftpo | Gliosis | Yes |
| 13 | 10.8 | F | 6.9 | R | fp | ftp | t | FCD | No |
| 14 | 14.1 | M | 8.3 | R | p | p | ftp | FCD | No |
| 15 | 2.7 | M | 2.4 | R | fto | ftpo | f | TSC,gliosis | No |
| 16 | 13.3 | M | 4.4 | R | ftp | ftpo | f | Gliosis | Yes |
| 17 | 2.9 | F | 1.4 | L | t | ftpo | fp | Gliosis | Yes |
| 18 | 13.8 | F | 9.9 | R | t | fpo | ft | Gliosis | No |
| 19 | 5.7 | F | 4.5 | L | t | ft | po | Gliosis | Yes |
| 20 | 16.2 | F | 14.4 | R | ftpo | none | none | Gliosis | No |
| 21 | 11.6 | F | 5.8 | R | t | ftp | tpo | FCD | Yes |
| 22 | 1.8 | M | 1.3 | R | to | tpo | none | mild MCD | Yes |
| 23 | 17 | F | 16.4 | L | f | o | f | Gliosis | Yes |
| 24 | 12.2 | M | 7.3 | L | t | t | fto | Gliosis | No |
| 25 | 10.7 | F | 10.4 | L | tpo | ftpo | f | FCD | Yes |
| 26 | 3.3 | M | 1.3 | R | fp | fp | ftp | Gliosis | Yes |
| 27 | 13.4 | M | 6.2 | L | t | ftp | none | mild MCD | No |
| 28 | 11.9 | M | 9 | R | tpo | p | tp | Gliosis | Yes |

| Pt. No. | Age (years) | Gender | Epilepsy duration (years) | Surgery side | ECoG Onset lobe(s) | SPM hypo | SPM hyper | Histology | Seizure Free |
|---|---|---|---|---|---|---|---|---|---|
| 29 | 15.1 | M | 10 | L | t | none | f | Gliosis | Yes |
| 30 | 14.3 | M | 8.5 | L | to | to | none | Gliosis | Yes |
| 31 | 11.8 | M | 8.9 | R | p | fpo | tp | FCD | Yes |
| 32 | 16.5 | M | 12.4 | L | t | t | none | Gliosis | Yes |
| 33 | 13.5 | F | 11.4 | L | t | ftp | none | Gliosis | No |
| 34 | 1.2 | M | 1.1 | L | t | none | t | FCD | Yes |
| 35 | 2 | F | 1.5 | L | ftp | tp | none | Gliosis | Yes |
| 36 | 2 | M | 0.6 | R | ftpo | to | tp | Gliosis | Yes |
| 37 | 1.2 | M | 0.8 | L | ftpo | ftpo | f | Gliosis | Yes |

SPM=statistical parametric mapping, ECoG=electrocorticography, M=male, F=female, FCD=focal cortical dysplasia, MCD=malformation of cortical development, OG=Oligodendroglioma, GG=Ganglioglioma, TSC=Tuberous Sclerosis Complex, L=left, R=right, f=Frontal, t=temporal, p=parietal, o=occipital

**Table 2**

Percentage of patients whose FDG metabolic abnormalities correspond to at least one electrode of ECoG-defined SOZ and interictal spiking area.

| | SOZ | | | | | Interictal spiking | | | | |
|---|---|---|---|---|---|---|---|---|---|---|
| **Hypometabolic** | **t−score≤−2** | **−2.5** | **−3.0** | **−3.5** | **−4.0** | **t−score≤−2** | **−2.5** | **−3.0** | **−3.5** | **−4.0** |
| **<10mm** | 68 | 66 | 55 | 40 | 32 | 87 | 84 | 71 | 61 | 53 |
| **15mm** | 79 | 71 | 61 | 42 | 32 | 89 | 87 | 74 | 63 | 55 |
| **20mm** | 79 | 71 | 63 | 42 | 34 | 89 | 87 | 74 | 63 | 55 |
| **25mm** | 79 | 71 | 63 | 45 | 34 | 89 | 87 | 76 | 66 | 58 |
| **30mm** | 79 | 71 | 63 | 53 | 34 | 92 | 87 | 79 | 68 | 61 |
| **Hypermetabolic** | **t−score≥2** | **2.5** | **3.0** | **3.5** | **4.0** | **t−score≥2** | **2.5** | **3.0** | **3.5** | **4.0** |
| **<10mm** | 42 | 26 | 13 | 5 | 5 | 61 | 45 | 21 | 8 | 5 |
| **15mm** | 42 | 26 | 13 | 10 | 10 | 61 | 45 | 26 | 11 | 8 |
| **20mm** | 45 | 34 | 16 | 10 | 10 | 61 | 53 | 32 | 11 | 8 |
| **25mm** | 45 | 37 | 21 | 10 | 10 | 63 | 55 | 37 | 13 | 8 |
| **30mm** | 47 | 37 | 21 | 10 | 10 | 63 | 55 | 37 | 16 | 13 |